Ion Channels and Genetic Diseases

Society of General Physiologists • 48th Annual Symposium

Edited by

David C. Dawson

and

Raymond A. Frizzell

Chapter 1

Models of Protein Structure

Structural Models of Na$^+$, Ca^{2+}, and K$^+$ Channels

H. Robert Guy and Stewart R. Durell

Laboratory of Mathematical Biology, DCBDC, National Cancer Institute, National Institutes of Health, Bethesda, Maryland 20892

The most serious impediment in the field of ion channel research is the lack of detailed, experimentally determined structural models. These structures are vital for understanding how channels function, how drugs and toxins modulate these functions, and how naturally occurring genetic mutations lead to disease. Unfortunately, the very nature of membrane-bound ion channel proteins makes them extremely difficult to study by crystallographic and NMR methods. As a confounding factor, funding agencies have been reluctant to sponsor these long-term structure determination projects, which admittedly have uncertain futures.

In light of these problems, a large multidisciplinary effort has arisen to determine structural information about ion channels using more accessible, albeit less certain methods. Our contribution to this process has been to combine the available experimental data with structure prediction principles to develop molecular models of the ion channel proteins. This is an iterative procedure, where the models are used to suggest further experiments, and the resulting data are used to refine the models. For example, mutagenesis experiments have been very effective in verifying many features of the early voltage-gated channel models, such as which sequence segments span the membrane and form the voltage sensor, inactivation gate, selectivity filter, and ligand binding sites (Guy and Durell, 1994). Likewise, results of mutagenesis experiments have been instrumental in developing our latest refinements of the outer vestibules and ion-selective portions of K$^+$, Na$^+$, and Ca^{2+} channels. Here we present these latest models and new models of the entire transmembrane and outer portions of the inward-rectifying, ROMK1 channels.

Na$^+$ and Ca^{2+} Channel Outer Vestibules and Ion-selective Regions

The mutagenesis experiments described below have confirmed our prediction that the P segments (also called SS1 and SS2 in Na$^+$ channels and H5 in K$^+$ channels) form the inner pore and ion-selective filter of K$^+$, Na$^+$, and Ca^{2+} channels. In our first models of Na$^+$ channels (Guy and Seetharamulu, 1986), we suggested that the P segments of repeats I to III each form a short α-helical hairpin, and that the negatively charged faces of the second helix form the ion-selective lining of the pore. Since then we have considered many other possibilities: e.g., a helix followed by a β strand (Guy, 1990; Guy and Conti, 1990), a β hairpin that assembles into a β barrel (Durell and Guy, 1992), and a helix followed by a random coiled structure in K$^+$ channels (Guy and Durell, 1993). Recent analysis of the expanded set of P segment sequences and new experimental data from Na$^+$ and Ca^{2+} channels have lead us to return to the original helical hairpin motif. However, now the ion-selective region and tetrodotoxin (TTX) and saxitoxin (STX) binding site is postulated to be formed by the central residues that link the two helices and/or by the residues that initiate the second helix. In addition, the helices are no longer postulated to be oriented

parallel to the pore's axis, but rather are tilted so that they form a cone-shaped outer vestibule.

A representation of P segment sequences is shown in Fig. 1. To simplify the comparison of homologous sequences, the numbers have been adjusted to match the aligned prolines of the K^+ channels and of repeats II and IV of the Ca^{2+} channels. In the Ca^{2+} channel sequences, the best conserved residues among the four repeats are the threonine at position 12p (T12p), the glutamic acid at position 14p (E14p), and the tryptophan at position 16p (W16p). It is therefore not surprising that mutagenesis experiments have identified the residues at position 14p to be a primary determinant of the ion selectivity. In particular, mutation of the positively charged K14p of repeat III and the uncharged A14p of repeat IV in Na^+ channels to negatively charged glutamic acid makes the pore properties resemble those of the


```
              1p    5p   10p        15p   20p
Na   I     FDTFswAFLaLFRlMT----qDfWEnLyqlT
Na   II    mhdFfhSFLiVFRVLc----GEwiETmwDcM
Na   III   FDNVGlgyLSLLQVAT----FkGWmDIMYAA
Na   IV    FeTFGnSMIcLFQitT----saGWdgLLapi
Ca   I     FDNFGfSMLtVyQCiT----mEGWtDVLYwv
Ca   II    FDNFPQALISVFQVLT----GEdWnsVMYng
Ca   III   FDNVlSAMmSLFTVsT----FEGWPqLLYrA
Ca   IV    FqTFPQAVLLLFRCAT----GEaWqEILLAc
cGMP       ARkYVySLYWStlTLTTi--GEtpPpVrDse
K   AKT1   wmrYVTSMYWSITTLTTVGYGDlhFVnTkEM
K   EAG    ksmYVTALYFtMTCMTsVGfGnVaAETdnEK
K   Shak   FkSiPdAPwWavVTMTTVGYGDmtFVgfwGK
K   mSlo   AlTTwecVYLLMVTMSTVGYGDVyAkTTLGR
K   Eco    pRSlmTAFYFSIETMSTVGYGDivFVsesAR
K   ROMK1  ingmtSAFLFSLETqvTIGYGfrfvTeqcAT
              1p    5p   10p   15p   20p   25p
```

Figure 1. Sequences of P segments from a Na^+ rat brain channel (Noda et al., 1986), a skeletal muscle Ca^{2+} channel (Tanabe, Takeshima, Mikami, Flockerzi, Takahashi, Kangawa, Kojoma, Matsuo, Hirose, and Numa, 1987), a cyclic nucleotide-gated channel (cGMP) (Kaupp, Niidome, Tanabe, Terada, Bonigk, Stühmer, Cook, Kangawa, Matsuo, Hirose, Miyata, and Numa, 1989), KAT1 *Arabidose* K^+ channel (Anderson, Huprikar, Kochian, Lucas, and Gaber, 1992), EAG K^+ channel (Warmke, Drysdale, and Ganetzky, 1991), *Shaker* voltage-gated K^+ channel (Tempel, Papazian, Schwarz, Jan, and Jan, 1987), mSlo Ca^{2+}-activated K^+ channel (Butler et al., 1993), a putative K^+ channel from *E. coli* (Milkman and McKane-Bridges, 1993), and an inward-rectifying K^+ channel, ROMK1 (Ho, Nichols, Lederer, Lytton, Vassilev, Kanazirska, and Herbert, 1993). Na^+ and Ca^{2+} channel segments are numbered beginning with the first proline in the repeats II and IV of Ca^{2+} channels (*top*) and K^+ channel segments beginning with the first proline in *Shaker* P segment (*bottom*). Residues that occur in three or more sequences in this alignment are bold, those that occur in two sequences are in normal upper case, and those that occur in only one sequence are in lower case. Alignment of Na^+ and Ca^{2+} with K^+ channels is difficult and ambiguous.

native Ca^{2+} channels (Heinemann, Terlau, and Imoto, 1992a). That is, the permeability of the mutant channels to Na^+ is blocked by low concentrations of Ca^{2+}, and at higher concentrations the channels become permeant to Ca^{2+}. Likewise, mutating any of the E14p's of Ca^{2+} channels to lysine makes the pore properties similar to those of Na^+ channels (Kim, Morii, Sun, Imoto, and Mori, 1993; Mikala, Bahinski, Yatani, Tang, and Schwartz, 1993; Yang, Ellinor, Sather, Zhang, and Tsien, 1993). However, the exact effect of mutating the E14p's of Ca^{2+} channels to lysine or glutamine depends upon which repeat is altered. Thus, in spite of the sequence similarity of the four repeats, the pore is functionally asymmetric. In addition to this, other experiments have shown that calcium channels appear to have two Ca^{2+} binding sites near the extracellular surface (Almers and McCleskey, 1984; Hess and Tsien, 1984). To explain these results, Yang et al. (1993) suggested that some of the

14p glutamic acids form one Ca^{2+} binding site near the extracellular entrance of the pore and others form an additional site farther down inside the pore. In our calcium channel models, the asymmetry and multiple binding sites were approached by considering the differences in the central residues which link the helices of the P segment hairpins (see Fig. 1). For example, glycines occur at position 13p in repeats II and IV and at position 15p in repeats I and III. Due to their enhanced flexibility, glycine residues occur most commonly in the coil and turn segments of proteins (Chou and Fasman, 1978). In addition, highly conserved gylcines tend to be involved in backbone folds that can not be accommodated by the other, more conformationally restricted residue types (Overington, Donnelly, Johnson, Sali, and Blundell, 1992). In the P segment model, repeats II and IV have only two residues, T12p and G13p, linking the helices; whereas, repeats I and III have four nonhelical residues, 12p through 15p, linking the helices (see Fig. 2 *A*). In repeats I and III, residues 13p-16p are postulated to form a type II β turn. This corresponds with the position of the glycines in these repeats, which usually are at the third position of a type II β-turn (Rose, Gierasch, and Smith, 1985). A longer linking segment is also suggested in repeat III by the presence of the proline at position 17p, which is the second residue of the second helix in the model. Due to their unusual structure, proline residues inhibit helical formation in the residues preceding them, but often initiate helices in the residues that follow them (Chou and Fasman, 1978).

As shown in Fig. 2 *B*, the four P segment hairpin structures are assembled, with an approximate fourfold symmetry, about the axis of pore to form a cone-shaped outer vestibule. This model was also designed so that the residues which would be exposed to water in the vestibule are primarily hydrophilic, and the residues which are buried between the helices and the other transmembrane segments are hydrophobic. For the reasons described above, the negatively charged E14p carboxylate groups are made to form the selectivity filter, by being placed at the narrowest portions of the pore. E14p of repeats II and IV form a Ca^{2+} binding site near the extracellular entrance of the pore, and the E14p of repeats I and III form a second site farther down in the pore. In addition to differences in the backbone structure, side chain differences introduce additional asymmetry; e.g., in this model, Ca^{2+} may bind off the pore's axis to D17p of repeat I and E17p of repeat IV in the outer entrance of the selectivity filter and to D15p of repeat II in the inner entrance.

Unfortunately, the P segments of the Na⁺ channel are more difficult to model because their sequences differ more among the four repeats than they do for the Ca^{2+} channels. Thus, backbone conformations of the P segment from different repeats are likely to differ even more than in Ca^{2+} channels. Fortunately, however, more experimental data are available for Na⁺ channels than for Ca^{2+} channels. For example, not only have mutagenesis experiments indicated that the 14p residues of Na⁺ channels are crucial for ion selectivity (described above), but that the binding of TTX and STX depends strongly upon the identity of the 14p and 17p residues in all four repeats (Terlau, Heinemann, Stühmer, Pusch, Conti, Imoto, and Numa, 1991). Conversely, mutation of the residues at positions 9p, 13p, 16p, and 18p appear to have little effect on the binding of these toxins. Also, mutation of the F15p residue of repeat I to cysteine causes a decreased sensitivity to TTX and STX and an increased sensitivity to blockade by zinc (Backx, Yue, Lawrence, Marban, and Tomaselli, 1992; Heineman, Terlau, Stühmer, Imoto, and Numa, 1992*b*; Satin, Kyle, Chen, Bell,

Cribbs, Fozzard. and Rogart, 1992). In contrast, mutation of this residue to tyrosine has little effect.

Fig. 2 *D* displays one of several helical hairpin models we developed for the binding of TTX in Na⁺ channels. In accordance with the data described above, each model satisfies the criterion of having almost all of the polar atoms of the toxin
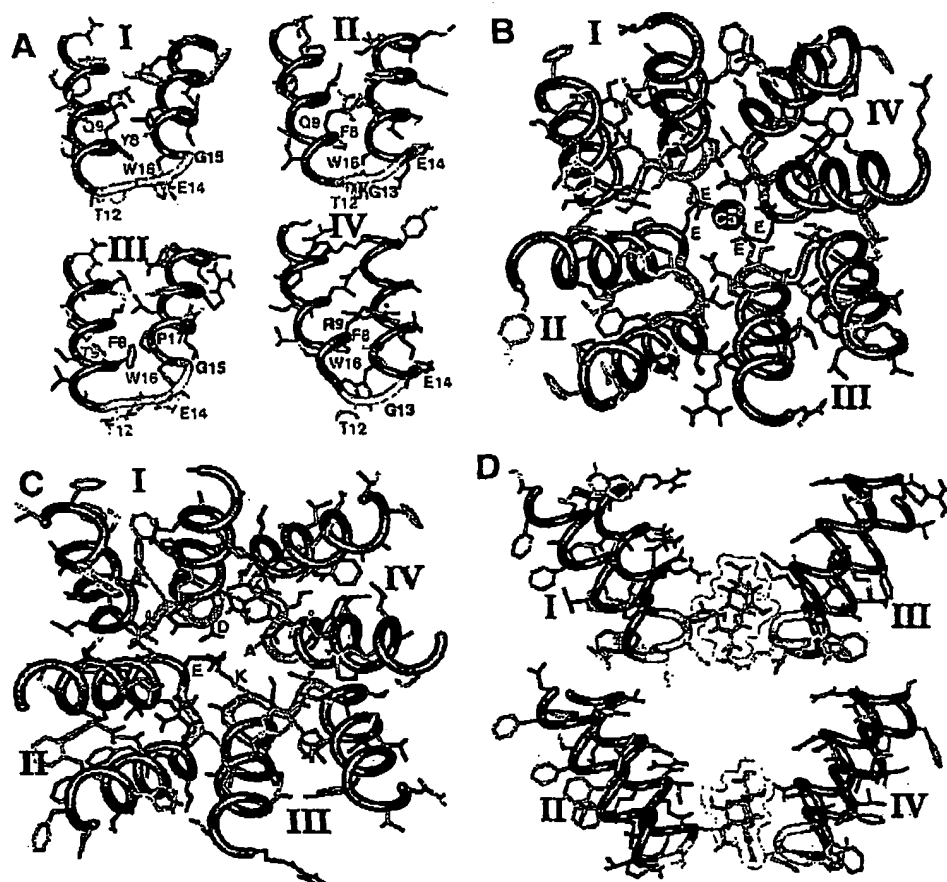

Figure 2. Models of Ca²⁺ and Na⁺ channel P segments. (*A*) Models of the four putative P segment helical hairpins of a Ca²⁺ channel viewed as from inside the channel. Top is extracellular. Lightly shaded portions are the putative nonhelical linking regions. (*B*) Model of the four Ca²⁺ channel P segments as assembled in the pore viewed from outside the cell. (*C*) Model of the four P segments of Na⁺ channel P segments viewed from outside the cell. (*D*). Side view of Na⁺ channel P segments with TTX (*outlined molecule*) bound in the outer entrance of the pore.

forming salt bridges or hydrogen bonds with the 14p and 17p residues of the P segments. Unfortunately, the positions of the helices, conformations of the connecting loops and side chains, and even the order of the repeats remains ambiguous in the Na⁺ channel model. It should be noted that Lipkind and Fozzard (1994) proposed an alternate model for the P segments where β hairpins are used instead of

helical hairpins. However, the models agree in the sequence location of the turn segments, which are likely the ion-selective region.

K⁺ Channel Outer Vestibules and Ion-selective Regions

The K⁺ channels are easier to model than the Na⁺ and Ca²⁺ channels because they are comprised of four identical subunits rather than four homologous repeats. Thus, it is more reasonable to assume that the channel has fourfold symmetry with respect to the pore's axis, which in turn reduces the number of possible conformations. In addition, there is considerably more mutagenesis data for the K⁺ channels than for the other types of channels. However, modeling of the K⁺ channel P segments is complicated by the recent findings of Heginbotham, Lu, Abramson, and MacKinnon (1994) which suggest that the ion selective region is not formed by any particular residue side chain, but rather by the polar atoms of the backbone. This also complicates using substitution-type mutagenesis experiments, which just switch side chain identities, for determining which particular residues are involved in ion selectivity. Assuming a hairpin motif, another complicating factor is that the segment of linker residues is substantially longer for the K⁺ channels than for the Na⁺ or Ca²⁺ channels (see Fig. 1). Finally, the highly conserved glycines at position 15p and 17p in the putative ion selective linker region are more difficult to model because they have considerably more conformational freedom than the other types of residues. However, it will be shown in the following sections how these seeming difficulties may actually provide clues to the structure of the channel.

Due to the ambiguities, we have developed a number of different models for the P segment structure of K⁺ channels. Despite the differences, they all share the following attributes, most of which have been predicted by mutagenesis and/or drug-binding experiments. These are (*a*) the 1p to 9p segment forms an α helix that is oriented such that residues 2p and 9p, which have been identified with tetraethylammonium (TEA) binding from the outside (see below), are accessible from the extracellular surface; (*b*) residue 20p, which is on the other end of the P segment, also forms part of the extracellular TEA binding site; (*c*) the backbone carbonyls of the highly conserved G15p-Y16p-G17p segment forms at least part of the ion-selective portion of the pore; (*d*) residues 11p, 12p and 14p, in the middle of the P segment, form at least part of the intracellular TEA binding site; and (*e*) the D18p residue of voltage- and calcium-gated K⁺ channels interacts with positively charged residues of charybdotoxin (CTX) when it is bound in the pore. The major differences among the models are in the conformation of the 10p to 20p region in the middle of the P segment sequence. In particular, the models of the pore structure have included four-stranded β barrels (spiraling right, left and straight up and down), short eight-stranded β barrels (formed from the linkers in β-hairpin conformations), a series of vertical β turns, and an extended structure in which the backbone has either a β-strand conformation or a conformation in which the backbone angles of the residues alternate between the values for right- and left-handed α helices (with the conserved 15p and 17p glycine residues assuming the left-handed conformation). We tentatively favor these extended models because they satisfy the experimentally determined criteria described below of having numerous K⁺ binding sites and a substantial distance between the intracellular and extracellular TEA binding sites and because they provide a role for the highly conserved glycine residues. The secondary structure predictions of the first α helix and the random coil for the central

region are supported by circular dichroism analysis of the isolated *Shaker* P segment in apolar solvent (Peled and Shai, 1993).

Sequence homology and mutagenesis data. Identification of which residues and regions of the sequence are conserved among different protein species is often useful in prediction of protein structure (see Guy and Durell, 1994). Conserved residues generally play important structural and/or functional roles in the protein. Elucidation of these roles is facilitated by correlating the conservation of known functional properties of different proteins with the conservation of the sequences. Fortunately for modeling efforts, there has been a rapid growth in the acquisition of K^+ channel sequences from a variety of families. These families include, voltage-gated, Ca^{2+}-activated, *Eag*, plant, bacterial, and Mg^{2+}-blocked inward-rectifying channels. Because all of the K^+ channels are by definition selective for K^+, comparison of the most distantly related sequences is useful for identifying which residues are essential for K^+ selectivity. For example, 9p-18p is by far the best conserved segment among the distantly related K^+ channel sequences. Within this segment, the Mg^{2+}-blocked inward-rectifying channels (ROMK1, IRK1, GIRK1, KATP) have only five residues (T10p, T13p, G15p, Y16p, and G17p) that are identical to those of most other K^+ channels (see Fig. 1). In addition, many of the residue substitutions are nonconservative; For example, the hydrophobic V9p, M11p, and M19p or V19p residues in the *Shaker* and *Slow-poke* sequences are replaced by the hydrophilic E9p, Q11p, and R19p residues in the ROMK1 sequence, and the negatively charged D18p residue in the *Shaker* and *Slow-poke* sequences is replaced by the hydrophobic F18p residue in the ROMK1 sequence. Of the five conserved residues just described, the two threonine residues are also found conserved in the sequences of the cyclic nucleotide-gated channels (see Fig. 1). Because the cyclic nucleotide-gated channels are nonselective among cations, these threonines are probably conserved for reasons unrelated to K^+ selectivity. Also, T10p, T13p, and Y16p are replaced by S10p, C13p, and F16p in the *Eag* K^+ channel sequence, which leaves the two glycines as the only residues conserved among all of the K^+ channel sequences. This suggests that these glycine residues are crucial for the K^+ selectivity of the channels.

The importance of the two conserved glycines for K^+ selectivity is also indicated by the mutagenesis experiments of Heginbotham et al. (1994), in which every position of the central region of the *Shaker* P segment was mutated one residue at a time. It was found that every residue other than G15p and G17p can be substituted without substantially altering the channels selectivity for K^+ over Na^+. Substitution of either glycine, however, greatly reduces the channel's selectivity among cations. Similarly, Heginbotham, Abramson, and MacKinnon (1992) were able to reproduce the nonselective properties of the cyclic nucleotide-gated channels by deleting the G15p and Y16p residues in the *Shaker* P segment, which is the same as the natural deletion between the two channel sequences (see Fig. 1). In particular, the mutated channel was permeant to both Na^+ and K^+ and was blocked by relatively low concentrations of Ca^{2+}. Likewise, the additional mutation of the D18p residue to E18p resulted in conduction properties similar to those of Ca^{2+} channels, which naturally have the a glutamic acid residue at this location and also lack the G15p and Y16p residues of K^+ channels (see Fig. 1).

These findings have important implications for the structure of the ion-selective portion of the pore. As described above, the mutagenesis results indicate that the highly conserved 15p and 17p glycine residues are the most influential in determining

the K+ selectivity. (It should also be noted that the hydroxyl group of T10p may also play a role in selectivity [Heginbotham et al., 1994]). Because glycine residues lack side chains, we modeled the selectivity filter, which is taken to be the narrowest portion of the pore and in direct contact with the cations, to be formed by the partial negatively charged carbonyl oxygens of the conserved G15p-Y16p-G17p residue backbones (Heginbotham et al., 1994). In addition, we make the assumption that the glycine residues were probably conserved by evolution because they are able to assume a conformation which is energetically unfavorable for other residue types, which is generally what is observed for the highly conserved gylcine residues in soluble proteins (Overington et al., 1992). For this reason, the ion-selective, central region of the P segment would likely not have a regular α helical or β strand conformation. Instead, our models of the K+ channels have this region of the P segment forming either a random or extended conformation (see Fig. 3).

Multiple K+ binding sites. Experimental studies have indicated that Ca2+-activated K+ channels may possess up to four K+ binding sites in their pore (Neyton and Miller, 1988). Assuming that the sites are arranged single file, this helps constrain the modeling by requiring a long, narrow pore structure. As shown in Fig. 3, this is accomplished by having the highly conserved, ion-selective region of the P segment in an extended conformation, oriented parallel to the axis of the pore. Two conformational extremes are illustrated. Fig. 3 *E* shows the pore when no ions are present, and thus, the amide groups are free to form interstrand hydrogen bonds. This four-stranded structure is very atypical, in that most β barrels have at least six strands which spiral around the axis in a right-handed fashion. However, the lack of interior side chains due to the one-residue–separated positions of the conserved G15p and G17p residues makes this narrow structure feasible. Fig. 3 *F* shows the other extreme, where the amide groups have rotated by 90° so that the carbonyl oxygens can interact with the ions in the pore. To accomplish this, the torsion angles of the residue backbones alternate along the strand between the values for left- and right-handed α helices. Once again, this is feasible due to the fact that the conserved glycine residues lack side chains and are thus able to assume left-handed helical conformations. The V14p and Y16p residues assume the normal right-handed helical torsion values. This peculiar conformation for the strands allows for all the carbonyl oxygens to point into the pore and form K+ binding sites. Two basic types of binding sites are imagined: one with the ion in the plane of four carbonyl oxygens, and one with the ion in between two planes of four oxygens each (thus, binding to eight oxygens all together). In these models, the pore's lining is envisioned to be a highly dynamic, polarizable structure whose precise conformation is influenced by the location and number of ions in the pore. The examples illustrated are the narrowest pores that we have modeled. The pore may be made larger by adding additional water modelcules.

TEA binding sites. The prediction of a long, extended pore structure is also supported by the data for TEA binding. Many of the different K+ channel pores are found to be blocked by TEA at two distinct sites; one accessible from outside the cell and the other from inside the cell. From the voltage dependency of binding, it is found that the TEA molecule need not traverse much, if any, of the transmembrane electric field to reach the extracellular site, and only transverses 20% of the field to reach the intracellular site (Miller, 1991). Although electrostatic repulsion between TEA ions at the two sites has been reported (Newland, Adelman, Tempel, and
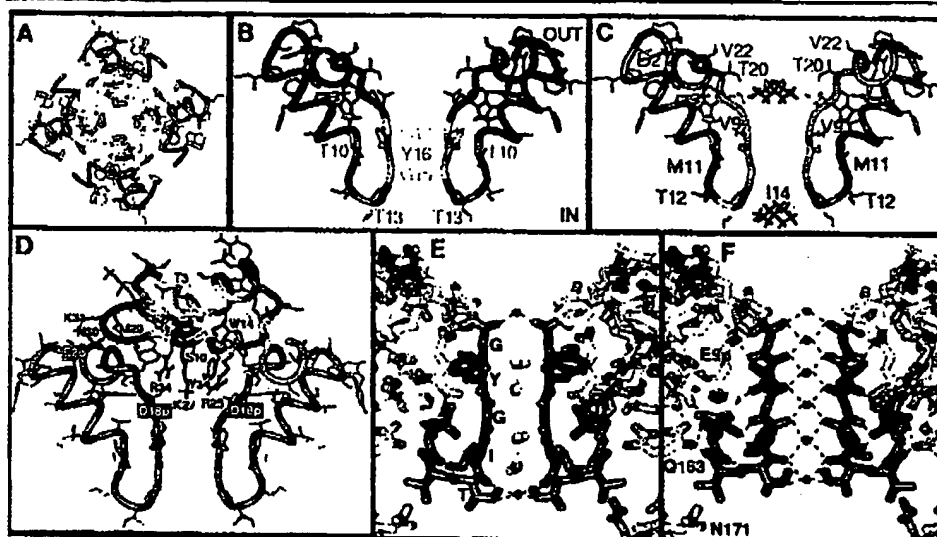
Figure 3. Models of *Shaker* K^+ channel P segments. (*A*) Assembly of four P segments to form outer vestibule and ion-selective region of the channel; view from outside the cell. Dark gray tubes are backbones of α helices; white tubes are random coil backbone. Side chain color code: gray=alkyl carbons, pink=uncharged oxygens, red=negatively charged oxygens, light blue=uncharged nitrogens, yellow=sulfurs. (*B*) Cross-section of outer vestibule and ion-selective region showing two P segments. View is the same as in *A* except monomers are rotated by 90°. Residues are colored coded according to how well they are conserved among distantly related K^+ channels: the number of residue types in all sequences are: yellow=1, orange=2, red=3, purple=4, blue=5. (*C*) Side view of P segments illustrating residues where mutations alter TEA binding from outside (*green*) and inside (*purple*) the cell. TEA molecules (*dark blue*) are ~15 Å apart. (*D*) Illustration of charybdotoxin (CTX) bound in the outer vestibule of a Ca^{2+}-activated mslo channel. CTX residues are colored according to how much mutations affect the off rate of binding: red=large effect, yellow=moderate effect, green=little or no effect. Crucial CTX residues are labeled black and negatively charged channel residues are labeled white. (*E and F*) Side view of putative ion-selective portion of ROMK1 channel in two extreme conformations. In *E*, residues 14p-16p have a β conformation and the pore is filled with water molecules (*pink and white*). In *F*, residues I14p and Y16p have a right handed α type conformation, G15p and G17p have a left handed α type conformation and the pore is filled with K^+ ions (*cyan*). The actual pore is envisioned to be a highly dynamic structure that exists between these extremes most of the time. Q163 and N171 are residues on M2. All backbone atoms are shown. Color code: black=carbons of 10p-17p, white=carbons of other segments, pink=uncharged oxygens of backbone or side chain, red=negatively charged side chain oxygens, light blue=uncharged nitrogens, cyan=potassium ions, red dashed lines=salt bridges, black dashed lines=hydrogen bonds.

Almers, 1992), the fact that they are separated by 80% of the transmembrane electric field indicates a considerable separation distance.

Fig. 3 *C* shows the positions of residues in our model where mutations alter TEA binding at the extracellular (MacKinnon and Yellen, 1990; De Biasi, Kirsch, Drewe, Hartmann, and Brown, 1993) and intracellular (Yellen, Jurman, Abramson, and MacKinnon, 1991; Hartmann, Kirsch, Drewe, Taglialatela, Joho, and Brown, 1991; Choi, Mossman, Aubie, and Yellen, 1993) sites. The 20p residues from the four

subunits were positioned near the extracellular entrance to the pore so that when they are tyrosines or phenylalanines their aromatic groups form much of the TEA binding site, as suggested by Heginbotham and MacKinnon (1992). As described above, the extended structure of the pore maximizes the distance between the 14p and 20p residues, which are known to affect intracellular and extracellular TEA binding, respectively. The experimental data for the mutation of the 9p residue to histidine (De Biasi et al., 1993) is especially interesting because it alters the effects of extracellular TEA, zinc, histidine reagents, and changes in pH even though it is close in sequence to the M11p and T12p residues, where mutations affect the binding of intracellular TEA. In the models, the 9p residue, which is a valine in the *Shaker* and *Slow-poke* sequences, is buried in the nonpolar interior of the protein near the extracellular entrance to the pore. In the inward rectifier (ROMK1) the 9p residue is a buried glutamic acid; however, it is able to form neutralizing hydrogen bonds with the amide groups of four proximal residues in the model (see Fig. 3 *F*). Although the 9p residue is not directly in the pore lining or TEA binding site, as suggested by DeBiasi et al. (1993), it is in a crucial position such that the nonconservative mutation to histidine could easily affect the pore's structure and properties, as described above. The possibility that this mutation alters the backbone conformation of the channel is suggested by the finding that the mutation of the 9p residue to histidine also effects the channel's activation gating kinetics (De Biasi et al., 1993). Mutagenesis experiments also indicate that 2p is sufficiently near the extracellular TEA binding site to affect TEA binding by an indirect electrostatic mechanism (MacKinnon and Yellen, 1990). In analogy to the Na⁺ and Ca²⁺ channel models, we have modeled the K+ channel 1p-10p segment as an α helix. This model has the advantage of placing 2p and 9p relatively near each other on the face of the helix that is postulated to form part of the lining of the outer vestibule.

CTX binding. Docking of a charybdotoxin (CTX) molecule into the outer vestibule model was used to constrain the orientations of the helical portions of the P segments that are postulated to form the outer vestibule of the channel models. CTX is a scorpion toxin peptide that is known to block the extracellular entrance of some voltage-gated and Ca²⁺-activated K⁺ channels (Anderson, MacKinnon, Smith, and Miller, 1988; MacKinnon and Miller, 1988). Fortunately, the three-dimensional structure of the peptide in solution has been determined by NMR (Bontems, Gilquin, Roumestand, Menez, and Toma, 1992). Mutation of the positively charged K27 of CTX to a neutral residue has been shown to reduce the overall binding affinity and eliminate the ability of extracellular CTX to compete with intracellular K⁺ (Park and Miller, 1992). This strongly suggests that the positively charged ammonium group of K27 normally reaches into one of the K⁺ binding sites in the ion-selective region of the pore. As depicted in Fig. 3 *D*, the K27 CTX side chain is positioned inside the ring of the four negatively charged D18p residues of the P segments. This orientation for the CTX molecule is also supported by the finding that mutation of the S10, W14, R25, M29, N30, R34, and Y36 residues, which are on the same face of the CTX molecule as K27, significantly affect the dissociation rate from Ca²⁺-activated K⁺ channels. Likewise, nonconservative mutations of residues on the opposite side of the CTX molecule have little effect on the dissociation rate (Stampe, Kolmakova-Partensky, and Miller, 1994). In the model shown in Fig. 3 *D*, the positively charged R25 and R34 residues of CTX join with the K27 residue to form salt bridges with the four D18p residues. In addition, the K11 and K31 residues of

CTX form salt bridges with the E2p residues of adjacent subunits on the periphery of the outer vestibule. This interaction is supported by the finding that in the *Shaker* channel the mutation of D2p to asparagine eliminates the binding of CTX (MacKinnon and Yellen, 1990). Also in the model, the aromatic F2 and W14 residues of CTX bind at the beginning of the second helix of opposite subunits and interact with the Y20p and K22p residues of the P segments. Aromatic residues are known to have favorable interactions with other aromatics (Burley and Petsko, 1985) and with positively charged residues in known protein structures. Thus, CTX can dock into the model of the outer vestibule in a manner in which the interactions between the toxin and pore are highly complementary and consistent with the experimental findings.

Inward Rectifying K⁺ Channels

A major shortcoming of the models described so far is that they lack the surrounding transmembrane segments (S1–S6), which would likely influence the predicted conformations of the P segments. Although we have attempted to make atomic-scale models for the surrounding segments of voltage-gated (Durell and Guy, 1992) and Ca^{2+}-activated K^+ channels, the structures are too large to predict with much certainty. However, the situation is simplified for the inward-rectifying and homologous K^+ channel proteins, which probably have only two transmembrane helices (M1 and M2) per subunit in addition to the P segments.

Fig. 4 displays the model of the M1, M2, extracellular linkers and P segments of the ROMK1 channel. The procedures used to build the models has been described previously (Durell and Guy, 1992). In developing these models, we attempt to optimize the following interactions:

(a) Side chain-water interactions. Polar residues are made to contact other polar residues or the solvent.

(b) Side chain-lipid interactions. Nonpolar residues are either buried in the protein or made to be in contact with the alkyl chains of the membrane.

(c) Side chain-side chain interactions. A disulfide bride is formed between C121 and C153. Salt bridges are formed from D108 and E111 to R147, from D116 and E123 to R118, and from E152 to H106. Hydrogen bonds are formed between S130 and E153, Y100 and S135, S135 and S164, and W92 and Q139. A cluster of aromatic side chains is formed by W92, F95, W99, Y100, F134, Y144, F146, and F148 (see Fig. 4, *C* and *E*).

(d) Backbone hydrogen bonds. Virtually all backbone polar atoms are required to form hydrogen bonds. Most backbone polar atoms that are within regular secondary structures, i.e., α or 3_{10} helices or β sheets form hydrogen bonds to other backbone atoms. At the ends of helices or in "random coil" segments some of these atoms may hydrogen bond to side chain atoms, e.g., K107 interacts with the COOH terminal of M1, D108 and T139 with the NH_2 terminal of the first P-segment helix, T133, Q139 and Q164 with the COOH terminal of this helix, Q164 to the loop region that follows it, E137 with the pore-lining segment and the NH_2 terminal of the 3_{10} helix postulated to link the lining to M2, and T119 with the NH_2 terminal of a surface helix in the M1-P linking segment (see Fig. 4 *C*). The M1-P linking segment is postulated to have a random coil segment located on the extracellular surface of the protein where some unpaired backbone polar atoms hydrogen bond to water. Within the pore, some backbone oxygens may interact with ions (see Fig. 3 *F*). The putative random coil segments contain proline and glycine residues that tend to disrupt

helices and β sheets, whereas the putative helices do not contain these residues except for prolines at some of the NH₂ terminals where they are energetically favorable.

(*e*) Residue packing. The structure is modeled so that the atoms within the protein pack tightly together with no large cavities within the protein (see Fig. 4, *D* and *E*).

(*f*) Torsion angles. Residues are modeled with backbone and side chain torsion angles that occur commonly in known protein structures.
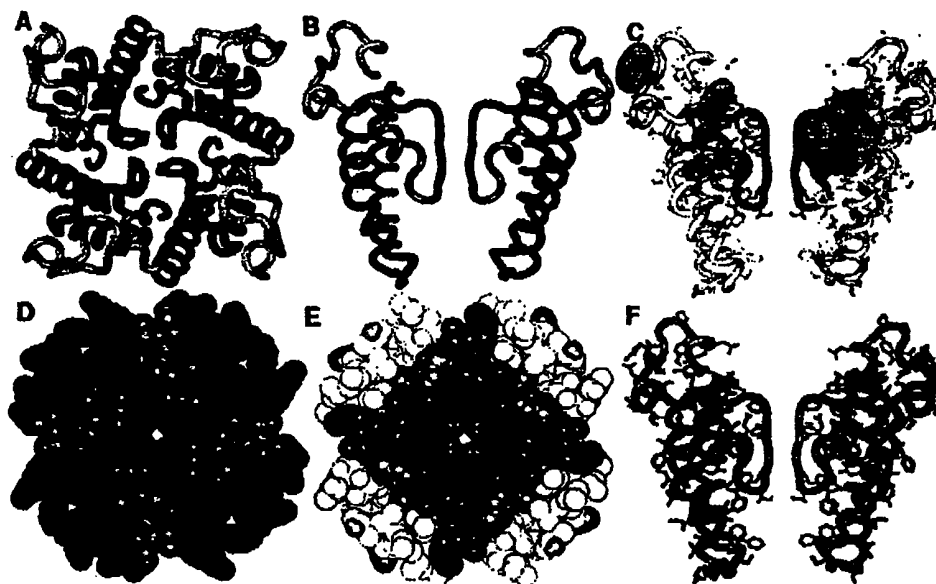

Figure 4. Model of transmembrane and extracellular portions of ROMK1 channel. (*A*) View from outside and (*B*) side view of backbone structure. Segments are color coded as: green =M1, yellow=M1-P extracellular linker, orange=P1, red=P2, purple=P-M2 linker, blue=M2. (*C*) Side view illustrating energetically favorable interactions. Shaded area color code: yellow=disulfide bridge, red=salt bridges, blue=side chain–side chain hydrogen bonds, cyan=side chain–backbone hydrogen bonds, purple=aromatic cluster. Gray backbone=P segment, white backbone=other segments. Polar side chain atoms colored as in Fig. 3 *A*. (*D* and *E*) Space-filled model of channels cross-section through the P segments illustrating tight packing. (*D*) Colored by segments as in *A* and *B*. (*E*) Colored as in *C* but with aromatic side chain carbon atoms colored purple in P and lavender in other segments. (*F*) Side view illustrating extent of sequence conservation. Yellow residues are identical in all K+ channel families except *Eag*. Color code for number of residue types in multisequence alignment of inward rectifying K+ channels: orange=1, red=2, purple=3, blue=4, gray≥5.

(*g*) Sequence conservation. Special attention is placed on whether a residue is conserved in the family of sequences (Guy and Durell, 1994). As is generally observed for known soluble and transmembrane protein structures, the poorly conserved polar and nonpolar residues are put in contact with either the solvent or the lipid, respectively (see Fig. 4 *F*). In contrast, the conserved residues are used for important structural and/or functional purposes. For example, the putative selectiv-

ity filter region is the most highly conserved part of the protein among all K^+ channels. In addition, many of the energetically favorable side chain–side chain and side chain–backbone interactions described above involve residues that are highly conserved within the family of K^+ channels that includes ROMK1.

The most noteworthy aspect of the ROMK1 model is that, beginning with the backbone structure of P segments developed from very distantly related K^+ channels, a model that satisfies all our criteria described above could be made of all the protein segments surrounding the P segment. Although the model of the pore formed by M1 and M2 in the intracellular half of the transmembrane region is more ambiguous, one aspect is consistent with recent experimental findings. N175 has been shown to be involved in the voltage-dependent blockade of ROMK1 by magnesium (Lu and MacKinnon, 1994). This effect has been postulated to be caused by an electrostatic effect. In our models, this residue is on the lining of the pore just beyond the end of the P segment where one might expect magnesium to bind (see Fig. 3 *E*).

Summary

The structure determination of voltage-gated channels by the combination of molecular modeling and mutagenesis experiments is a long term, iterative process. As such, the models should be considered as a work in progress, with changes expected as more data becomes available. The primary role of the models is that they assimilate the known data and provide ideas for further experiments to elucidate the real structures. Although the models presented here have already gone through two or three cycles of development and testing, many aspects remain tentative. Perhaps the most significant result so far is that the P segment was experimentally confirmed to form the ion-selective part of the channel. In a subsequent cycle of testing and modeling, the specific residues responsibility for Na^+ and Ca^{2+} selectivity have been identified and the selectivity filter of K^+ channels is now predicted to be formed not by the side chains, but rather by the carbonyl oxygens of the conserved Gly-Tyr-Gly sequence backbone. As another example, the 9p residue of the P segment of K^+ channels was originally modeled as either being buried in the protein or accessible from inside the cell only. However, once mutation of this residue to histidine was found to affect blockade by extracellular TEA, protons, Zn^{2+} and histidine reagents (DeBiasi et al., 1993), the models were updated to have this and the hydrophilic residues in the first part of P form a helix that comprises part of the extracellular, outer vestibule of the pore. While this motif was used also for Na^+ and Ca^{2+} pore models (see Fig. 2) where the putative helices are amphipathic, it remains to be verified. Modeling of the size and shape of the outer vestibule of K^+ channels was also aided by the data for the binding of CTX in the extracellular entrance to the pore. Similarly, experiments with peptide toxins such as μ and Ω conotoxins may prove useful in modeling the outer vestibules of the Na^+ and/or Ca^{2+} channels.

While important advances have been made, it is important to realize that these approaches are still very new. In the future we are likely to see improvements on both the theoretical and experimental sides which will greatly advance the process. For example, as computational power increases and as methods to calculate protein-ligand interactions improve, it will likely become possible to accurately calculate the binding affinities of toxins such as TTX and STX to the model pore structures of Na^+ and Ca^{2+} channels and compare these with experimental values. This should help

discriminate between different pore motifs. Similarly, computational studies of the free energy of ion permeation, such as pursued by Roix and Karplus (1994) and Chiu, Novotny, and Jakobsson (1993), may also greatly assist in understanding the structure of the pore and the mechanisms that enable ion selectivity.

Of course, what we need most is hard structural data; the type obtained by x-ray crystallography, NMR and electron cryomicroscopy. Unfortunately, It is unlikely that high resolution structures of voltage-gated channels will be obtained anytime soon. One reason is that the expression systems needed to produce the necessary quantity of purified protein have only recently been developed (Santacruz-Toloza, Perozo, and Papazian, 1994; Spencer, Takenaka, Aiyar, Ngyen, Grissmer, Gutman, and Chandy, 1994), and many additional difficulties remain to be overcome. However, it may be possible to use synthesized peptide analogues of the P segment with or without other segments to make membrane-bound crystals or water soluble. In this case, structural models will be essential for deciding how to tether the P segments together, and how to make the analogues long enough to span the bilayer or water soluble.

References

Almers, W., and E. W. McCleskey. 1984. Non-selective conductance in calcium channels of frog muscle: calcium selectivity in a single-file pore. *Journal of Physiology.* 353:585–608.

Anderson, C., R. MacKinnon, C. Smith, and C. Miller. 1988. Charybdotoxin block of single Ca²⁺-activated K⁺ channels: effects of channel gating, voltage, and ionic strength. *Journal of General Physiology.* 91:317–333.

Anderson, J. A., S. S. Huprikar, L. V. Kochian, W. J. Lucas, and R. F. Gaber. 1992. Functional expression of a probable *Arabidopsis thaliana* potassium channel in *Saccharomyces cerevisiae. Proceedings of the National Adademy of Sciences, USA.* 89:3736–3740.

Backx, P., D. Yue, J. Lawrence, E. Marban, and G. Tomaselli. 1992. Molecular localization of an ion-binding site within the pore of mammalian sodium channels. *Science.* 257:248–251.

Bontems, F., G. Gilquin, C. Roumestand, A. Menez, and F. Toma. 1992. Analysis of side-chain orgainzation on a refined model of charybdotoxin: structural and functional implications. *Biochemistry.* 31:7756–7764.

Burley, S. K., and G. A. Petsko. 1985. Aromatic-aromatic interaction: a mechanism of protein structure stabilization. *Science.* 229:23–28.

Butler, A., S. Tsunoda, D.P. McCobb, A. Wei, and L. Salkoff. 1993 mSlo, a complex mouse gene encoding 'maxi' calcium-activated potassium channels. *Science.* 261:221–224.

Chiu, S.W., J.A. Novotny, and E. Jakobsson. 1993. The nature of ion and water barrier crossings in a simulated ion channel. *Biophysical Journal.* 64:98–108.

Choi, K. L., C. Mossman, J. Aubie, and G. Yellen. 1993. The internal quaternary ammonium receptor site of *Shaker* potassium channels. *Neuron.* 10:533–541.

Chou, P.Y., and G. D. Fasman. 1978. Empirical predictions of protein conformation. *Annual Review of Biochemistry.* 47:251–276.

De Biasi, M., G. E. Kirsch, J. A. Drewe, H. A. Hartmann, and A. M. Brown. 1993. Cesium selectivity conferred by histidine substitution in the pore of the potassium channel Kv 2.1. *Biophysical Journal.* 64:A341. (Abstr.)

Durell, S. R., and H. R. Guy. 1992. Atomic scale structure and functional models of voltage-gated potassium channels. *Biophysical Journal.* 62:238–250.

Guy, H. R. 1990. Models of voltage- and transmitter-activated channels based on their amino acid sequences. *In* Monovalent Cations in Biological Systems. C. A. Pasternak, editor. CRC Press, Boca Raton, FL. 31–58.

Guy, H. R., and F. Conti. 1990. Pursuing the structure and function of voltage-gated channels. *Trends in Neuroscience.* 13:201–206.

Guy, H. R., and S. R. Durell. 1993. Models of the slowpoke calcium-activated potassium channel. *Biophysical Journal.* 64:A228. (Abstr.)

Guy, H. R., and S. R. Durell. 1994. Using homology in modeling the structure of voltage-gated ion channels. *In* Molecular Evolution of Physiological Processes. D. Fambrough, editor. The Rockefeller University Press, NY. 197–212.

Guy, H. R., and P. Seetharamulu. 1986. Molecular model of the action potential sodium channel. *Proceedings of the National Academy of Sciences, USA.* 83:508–512.

Hartmann, H. A., G. E. Kirsch, J. A. Drewe, M. Taglialatela, R. H. Joho, and A. M. Brown. 1991. Exchange of conduction pathways between two related K^+ channels. *Science.* 251:942–944.

Heginbotham, L., and R. MacKinnon. 1992. The aromatic binding site for tetraethylammonium ion on potassium channels. *Neuron.* 8:483–491.

Heginbotham, L., T. Abramson, and R. MacKinnon. 1992. A functional connection between the pores of distantly related ion channels as revealed by mutant K^+ channels. *Science.* 258:1152–1155.

Heginbotham, L., Z. Lu, T. Abramson, and R. MacKinnon. 1994. Mutations in the K^+ channel signature sequence. *Biophysical Journal.* 66:1061–1067.

Heinemann, S. H., H. Terlau, and K. Imoto. 1992. Molecular basis for pharmacological differences between brain and cardiac sodium channels. *Pflügers Archiv.* 422:90–92.

Heinemann, S. H., H. Terlau, W. Stühmer, K. Imoto, and S. Numa. 1992. Calcium channel characteristics conferred on the sodium channel by single mutations. *Nature.* 356:441–443.

Hess, P., and R. W. Tsien. 1984. Mechanism of ion permeation through calcium channels. *Nature.* 309:453–456.

Ho, K., C. G. Nichols, W. J. Lederer, J. Lytton, P. M. Vassilev, M. V. Kanazirska, and S. C. Hebert. 1993. Cloning and expression of an inwardly rectifying ATP-regulated potassium channel. *Nature.* 262:31–38.

Kaupp, U. B., T. Niidome, T. Tanabe, S. Terada, W. Bonigk, W. Stühmer, N. J. Cook, K. Kangawa, H. Matsuo, T. Hirose, T. Miyata, and S. Numa. 1989. Primary structure and functional expression from complementary DNA of the rod photoreceptor cyclic GMP-gated channel. *Nature.* 342:762–766.

Kim, M.-K., T. Morii, L.-X. Sun, K. Imoto, and Y. Mori. 1993. Structural determinants of ion selectivity in brain calcium channel. *FEBS Letters.* 318:145–148.

Lipkind, G. M., and H. A. Fozzard. 1994. A structural model of the tetrodotoxin and saxitoxin binding site of the Na^+ channel. *Biophysical Journal.* 66:1–13.

Lu, Z., and R. MacKinnon. 1994. Electrostatic tuning of Mg^{2+} affinity in an inward-rectifier K^+ channel. *Nature.* 371:243–246.

Mackinnon, R., and C. Miller. 1988. Mechanism of charybdotoxin block of the high-conductance, Ca^{2+}-activated K^+ channel. *Journal of General Physiology.* 91:335–349.

MacKinnon, R., and G. Yellen. 1990. Mutations affecting TEA blockade and ion permeation in voltage-activated K^+ channels. *Science.* 250:276–279.

Mikala, G., A. Bahinski, A. Yatani, S. Tang, and A. Schwartz. 1994. Differential contribution by conserved glutamate residues to an ion-selectivity site in the L-type Ca^{2+} channel pore. *FEBS Letters.* 335:265–269.

Milkman, R., and M. McKane-Bridges. 1993. An *E. coli* homologue of eukaryotic potassium channels. Genebank entry ECOKCH.

Miller, C. 1991. 1990: Annus mirabilis of potassium channels. *Science.* 252:1092–1096.

Newland, C. F., J. P. Adelman, B. L. Tempel, and W. Almers. 1992. Repulsion between tetraethylammonium ions in cloned voltage-gated potassium channels. *Neuron.* 8:978–982.

Neyton, J., and C. Miller. 1988. Discrete Ba^{2+} block as a probe of ion occupancy and pore structure in the high-conductance Ca^{2+}-activated K^+ channel. *Journal of General Physiology.* 92:569–586.

Noda, M., T. Ikeda, T. Kayano, H. Suzuki, H. Takeshima, M. Kurasaki, H. Takahashi, and S. Numa. 1986. Existence of distinct sodium channel messenger RNAs in rat brain. *Nature.* 320:188–192.

Overington, J., D. Donnelly, M. S. Johnson, A. Sali, and T. L. Blundell. 1992. Environment-specific amino acid substitution tables: tertiary templates and prediction of protein folds. *Protein Science.* 1:216–226.

Park, C. S., and C. Miller. 1992 Interaction of charybdotoxin with permeant ions inside the pore of a K^+ channel. *Neuron.* 9:307–313.

Peled, H., and Y. Shai. 1993 Membrane interaction and self-assembly within phospholipid membranes of synthetic segments corresponding to the H-5 region of the *Shaker* K^+ channel. *Biochemistry.* 32:7879.

Rose, G. D., L. M. Gierasch, and J. A. Smith. 1985. Turns in peptides and proteins. *Advances in Protein Chemistry.* 37:1–109.

Roux, B., and M. Karplus. 1994. Moleucular dynamics simulations of the gramididin channel. *Annual Review Biophysics Biomolecuar Structure.* 23:731–761.

Santacruz-Toloza, L., E. Perozo, and D. M. Papazian. 1994. Purification and reconstitution of functional *Shaker* K channels assayed with a light-driven, voltage-control system. *Biophysical Journal.* 66:A343. (Abstr.)

Satin, J., J. W. Kyle, M. Chen, P. Bell, L. L. Cribbs, H. A. Fozzard, and R. B. Rogart. 1992. A mutant of TTX-resistant cardiac sodium channels with TTX-sensitive properties. *Science* 256:1202–1205.

Spencer. R. H., B. Takenaka, J. Aiyar, A. Ngyen, S. Grissmer, G. A. Gutman, and K. G. Chandy. 1994. Purification and biochemical characterization of a mammalizn K^+ channel protein, Kv1.3. *Biophysical Journal.* 66:A343. (Abstr.)

Stampe, P., L. Kolmakova-Partensky, and C. Miller. 1994. Intimations of K^+ channel structure from a complete functional map of the molecular surface of charybdotoxin. *Biochemistry.* 33:443–450.

Tanabe,T., H. Takeshima, A. Mikami, V. Flockerzi, H. Takahashi, K. Kangawa, M. Kojima, H.

Matsuo, T. Hirose, and S. Numa. 1987. Primary structure of the receptor for calcium channel blockers from skeletal muscle. *Nature.* 328:313–318.

Tempel, B. L., D. M. Papazian, T. L. Schwarz, Y. N. Jan, and L. Y. Jan. 1987. Sequence of a probable potassium channel component encoded at *Shaker* locus of *Drosophila. Science.* 237:770–775.

Terlau, H., S. H. Heinemann, W. Stühmer, M. Pusch, F. Conti, H. Imoto, and S. Numa. 1991. Mapping the site of tetrodotoxin and saxitoxin of sodium channel II. *FEBS Letters.* 293:93–96.

Warmke, J., R. Drysdale, and B. Ganetzky. 1991. A distinct potassium channel polypeptide encoded by the *Drosophila eag* locus. *Science.* 252:1560–1562.

Yang, J., P. T. Ellinor, W. A. Sather, J.-F. Zhang, and R. W. Tsien. 1993. Molecular determinants of Ca^{2+} selectivity and ion permeation in L-type Ca^{2+} channels. *Nature* 366:158–161.

Yellen, G., M.E. Jurman, T. Abramson, and R. MacKinnon. 1991. Mutations affecting internal TEA blockade identify the probable pore-forming region of a K^+ channel. *Science.* 251:939–942.

Nucleotide Domains in Transport ATPases: Structure-Function and Relationship to Disease

Philip J. Thomas, Young Hee Ko, Ponniah Shenbagamurthi, and Peter L. Pedersen

Laboratory of Molecular and Cellular Bioenergetics, Department of Biological Chemistry, The Johns Hopkins University, School of Medicine, Baltimore, Maryland 21205-2185

It is known that over 50 transport systems exist which exhibit putative ATP binding domains (Higgins, 1992). Collectively these are referred to as the ABC transporter supergene family. They are referred to also as M-type ATPases (Pedersen and Amzel, 1993) because of their structural similarity to the multidrug resistance protein (MDR-1 or P-glycoprotein), and in other cases as traffic ATPases (Doige and Ferro-Luzzi Ames, 1993). Among this class of transporters are MDR-1, MDR-2, CFTR, TAP 1 and 2, STE6, and over 25 bacterial transporters. Most have two nucleotide domains.

A major effort of this laboratory has been to understand structural-functional relationships within the nucleotide binding domains of transport ATPases. Specifically, the nucleotide binding domains of the CFTR protein (cystic fibrosis transmembrane conductance regulator) and the mitochondrial ATPase/ATP synthase complex (an F-type ATPase) have been extensively studied. To this end, we have overexpressed these domains in *Escherichia coli* (Garboczi, Hullihen, and Pedersen, 1988; Lee, Garboczi, Thomas, and Pedersen, 1990; Ko, Thomas, and Pedersen, 1993), chemically synthesized key regions containing the nucleotide binding consensus sequences (Thomas, Shenbagamurthi, Ysern, and Pedersen, 1991; Ko, Thomas, and Pedersen, 1994), and used both mutational analysis (Garboczi, Thomas, and Pedersen, 1990; Thomas, Garboczi, and Pedersen, 1992a) and biophysical approaches (Thomas, Shenbagamurthi, Sondek, Hulihen, and Pedersen, 1992c; Chuang, Gittis, Abeygunawardana, Pedersen, and Mildvan, 1994) including circular dichroism spectroscopy and NMR, to relate structure to function. In addition, experiments are underway in an attempt to crystallize one of these nucleotide domains.

Work described here will focus specifically on the CFTR protein as mutations within both of its nucleotide domains have been linked to cystic fibrosis. Progress made in this laboratory in the study of these two nucleotide domains will be briefly described.

CFTR is an integral membrane protein (Riordan, Rommens, Kerem, Alon, Rozmahel, Grzelczak, Zilenski, Lok, Plausic, and Chow, 1989) comprised within a single polypeptide chain of 1,480 amino acids (Fig. 1). The five major domains include two nucleotide binding folds (NBF1 and NBF2), a regulatory domain (R), and two transmembrane spanning regions (TMSs). The latter, at least in part, form a Cl^- channel that is believed to require, for optimal function, both ATP hydrolysis

(Anderson, Berger, Rich, Gregory, Smith, and Welsh, 1991) mediated by NBF1 and phosphorylation of the R domain mediated by protein kinase A and/or other cellular kinases (Tabcharani, Chang, Riordan, Hanrahan, 1991; Cheng, Rich, Marshall, Gregory, Welsh, and Smith, 1991). Over 200 different mutations in the gene encoding CFTR induce amino acid changes in the protein which in turn cause cystic fibrosis (Tsui, 1992). Most cause mild forms of the disease, whereas others, like ΔF508 CFTR, result in severe forms of the disease. Unfortunately, ~90% of all cystic fibrosis patients have been reported to have at least one ΔF508 allele (Kerem, Corey, Kerem, Rommens, Mariewicz, Levinson, Tsui, and Durie, 1990).

NBF1 spans a ~155 amino acid region of CFTR (residues 433–588) and includes a Walker A (GX$_4$GKT/S), a Walker B (RX$_{6-8}$h$_4$D), and so-called linker or C consensus (LSXGXR/K). The Walker A and B consensus are found in many nucleotide binding proteins (Walker, Saraste, Runswick, and Gay, 1982) including adenylate kinases, ATP synthases, the RecA protein, and all members of the ABC transporter superfamily (Higgins, 1992). The C consensus, however, appears to be a unique feature of the ABC transporter superfamily (Shyamala, Baichwai, Beall, and Ames, 1991).
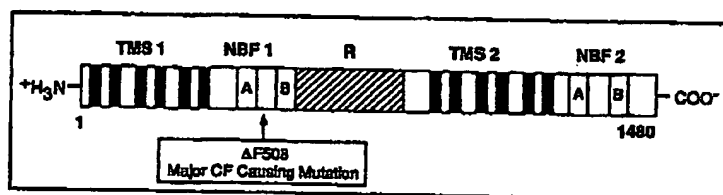

Figure 1. Presentation of the primary structure of the CFTR molecule. The relative positions of the five domains and the location of the ΔF508 mutation are depicted.

As no three-dimensional structural data is available for CFTR, or for any other member of the ABC transporter superfamily, NBF1 has been assumed to fold in a manner similar to adenylate kinase, the crystal structure of which is known (Schulz, Elzinga, Marx, and Schirmer, 1974; Sachsenheimer and Schulz, 1977). Fig. 2 *A* depicts the structural fold of adenylated kinase (Schulz et al., 1974; Sachsenheimer and Schulz, 1977). The region shown in black consisting of β strand/α helix/ β strand secondary structural organization is known to participate in binding ATP (Fry, Kuby, and Mildvan, 1986; Mildvan, 1986). Within this region the A consensus is located near the interface of the α helix and the loop (P loop). The A consensus is believed to interact directly with one or more of the three phosphate groups of ATP while the α helix may participate, in part, in binding the purine ribose moiety (Fry et al., 1986; Mildvan, 1989). The B consensus is located in a different region of adenylate kinase but, nevertheless, lies near the A consensus, and in some ATP binding proteins is believed to interact with Mg^{2+} (Story and Steitz, 1992).

Fig. 2 *A* shows also where the C consensus of NBF1 would be predicted to lie within the adenylate kinase fold. Significantly, its position resides downstream from the B consensus. Therefore, in three-dimensional space the A, B, and C consensus

regions are predicted to lie near one another. The C consensus evidently does not contribute to nucleotide binding per se.

Of the 19 major mutations within NBF1 that cause cystic fibrosis (Tsui, 1992), it is interesting to note that 13 lie within or near consensus regions (Fig. 2 *B*). The remaining six mutations lie within or near a hydrophobic β-strand insert where the major disease causing mutation ΔF508 occurs. Although this region was originally believed to be α helical in character (Hyde, Gill, Hubbard, and Higgins, 1990), four different programs for predicting secondary structure have been shown more recently to report β-strand character (Thomas et al., 1991). It is possible that in the folding pathway, a β strand is first to form which is then converted to an α-helix in the
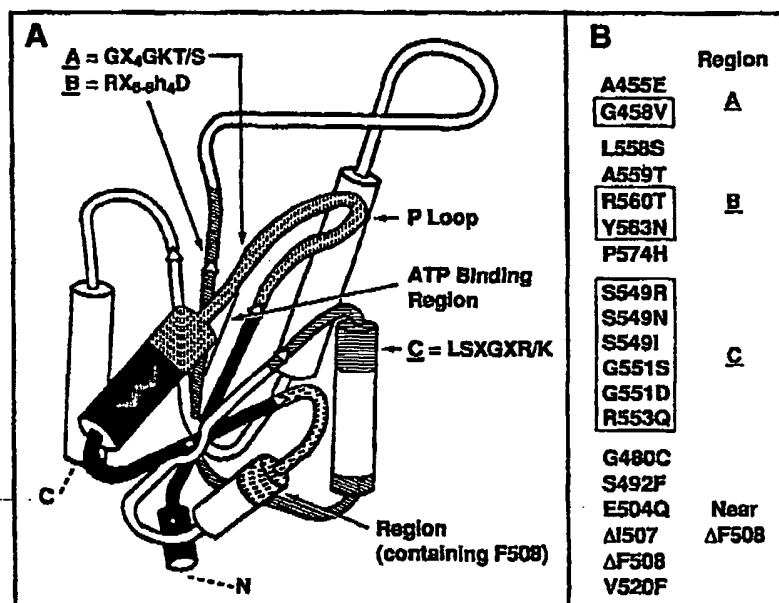

Figure 2. Adenylate kinaselike fold predicted in all members of the ABC transporter superfamily. Note the close proximity of the A, B, and C consensus to the ATP binding pocket, and CFTR to F508. Some investigators suggest that the rather hydrophobic insert containing F508 may interact with the membrane. (*B*) Mutations in NBF1 that cause cystic fibrosis. Boxes enclose mutations with consensus motifs.[1]

final folded structure. Whether or not this segment fits compactly within the adenylate kinaselike fold in NBF1 or projects out from it and into the membrane as speculated by some workers (Hyde et al., 1990; Baichwai, Liu, and Ames, 1993; Arispe, Rojas, Hartman, Sorscher, and Pollard, 1992) remains an interesting concept to be tested experimentally.

NBF2 spans a ~165 amino acid region of CFTR (residues 1219–1386) and includes the Walker A and Walker B consensus regions, as well as the C consensus.

[1] We are just completing the homology modeling of NBF1 and NBF2 in three dimensions based on known x-ray structures.

NBF2 exhibits considerable amino acid sequence homology to NBF1 (Smit, Wilkinson, Mansoura, Collins, and Dawson, 1993), and like NBF1, there are a number of mutations within the domain that result in cystic fibrosis (Tsui, 1992). However, none are as severe as that produced by the ΔF508 mutation in NBF1.

Results and Conclusions

In this section, experiments conducted over the past four years on the two nucleotide domains of the CFTR protein are briefly described. Experimental details and a more detailed discussion of most of this work can be found in (Ko et al., 1993, 1994; Thomas et al., 1991, 1992*b,c;* Thomas and Pedersen, 1993).

Preparations of NBF1 and NBF2 Peptides, and an NBF1 Fusion Protein

When we commenced this work, the CFTR protein had not been isolated, and there was no direct evidence that the two predicted nucleotide domains, NBF1 and NBF2
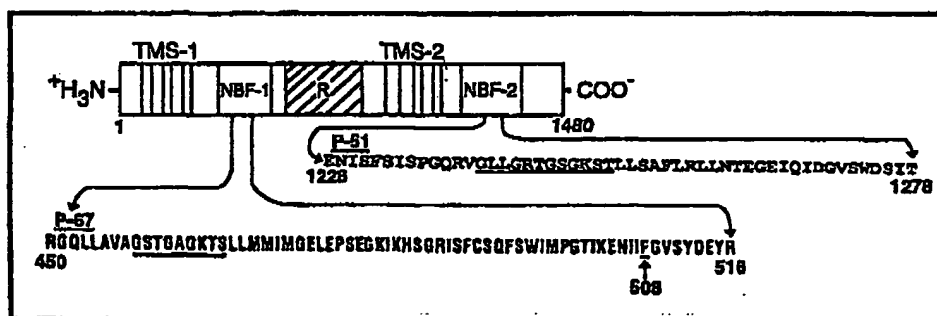

Figure 3. Peptides corresponding to the indicated regions of NBF1 and NBF2 of CFTR. These were chemically synthesized on a peptide synthesizer (model 430A, Applied Biosystems, Inc.) (Thomas et al., 1991; Ko et al., 1994). After hydrogen fluoride cleavage from the solid phase, the peptides were purified by reverse phase HPLC chromatography on a Waters C_{18} column. The Walker A consensus motif and F508 are underlined.

were in fact ATP binding domains. For this reason we designed, chemically synthesized, and purified both a 67 amino acid segment (P-67) of NBF1 (Thomas et al., 1991), which included the Walker A consensus motif and phenylalanine 508, and a 51 amino acid segment (P-51) of NBF2 (Ko et al., 1994) which also included the Walker A consensus motif (Fig. 3). These peptides correspond to the central core region of the adenylate kinase model where ATP is known to bind.

In addition to the above, we employed recombinant DNA technology to overexpress in *E. coli* the complete NBF1 domain (F433→S589) in fusion with the maltose binding protein (MBP) (Ko et al., 1993). The MBP protein was used both to facilitate purification on an amylose column and to provide a soluble MBP-NBF1 fusion product that might be suitable for crystallization. All three proteins, P-67, P-51 and MBP-NBF1, were subjected after preparation to a variety of purification tests as indicated in Table I. They were all judged to be >95% pure, and therefore, suitable for functional analysis.

Secondary structure. The three CFTR segments (P-67 from NBF1, MBP-NBF1, and P-51 from NBF2) were all shown by circular dichroism spectroscopy to exhibit significant secondary structure (Table II). Interestingly, the P-67 and P-51 peptides, which both span regions of NBF1 and NBF2 containing the Walker A consensus motif, distribute their secondary structural elements quite differently with P-67 exhibiting a high content of β-strand character relative to α helix and with P-51 exhibiting a high content of α-helical character relative to β strand. Neither P-67 nor P-51 showed an obvious propensity to form multimolecular structures, whereas the MBP-NBF1 construct, and not MBP alone, showed a propensity to form soluble organized polymeric structures which under high salt conditions partially dissociate and form microcrystals (see Fig. 8 of Ko et al., 1993). Clearly, a three-dimensional structure of the wild-type and ΔF508-NBF1 would be of particular significance in revealing the chemical details characterizing that region of NBF1 where the critical cystic fibrosis causing mutation lies. The formation of microcrystals of the MBP-NBF1 fusion protein represents an encouraging first step.

TABLE I

Yield and Criteria of Purity of NBF1 and NBF2 Components of CFTR

CFTR component	Region	Yield	Criteria of purity
P-67 from NBF1	R450 → P516	6–10 mg*	HPLC, SDS-PAGE, AA, and NH₂ terminus sequence analysis
MBP-MBF1	F433 → S589	~25 mg‡	HPLC, SDS-PAGE, AA, and NH₂ terminus sequence analysis
P-51 from NBF2	E1228 → T1278	6–10 mg*	HPLC, SDS-PAGE, AA, NH₂ terminus sequence and mass spectral analysis

*From ~300 mg of crude starting material.
‡Per liter cell culture.
AA, amino acid composition analysis.
See Ko et al. (1993, 1994) and Thomas et al. (1991) for details.

ATP binding. All of the above CFTR components prepared in this laboratory were found to bind the fluorescent nucleotide analogue trinitrophenyl-ATP (TNP-ATP) which could be displaced with ATP. Several control proteins including insulin failed to bind TNP-ATP. Table III shows that dissociation constants (K_ds) for ATP were all in the low mM range (0.30–1.8 mM) in analogy to numerous intracellular ATP-dependent enzymes. All CFTR components also bound TNP-ADP and to a much lesser extent TNP-AMP. Mg^{2+} was not necessary for nucleotide binding nor did it appreciably affect K_d values for all of the above CFTR components.

The studies described above demonstrate that NBF1 and NBF2 do interact with both ATP and ADP.

Effect of the ΔF508 mutation on the structure and function of the NBF1 peptide and on the MBP-NBF1 fusion protein. About 90% of all cystic fibrosis patients have been reported to have at least one ΔF508 CFTR allele (Chuang et al., 1994). Therefore, it was important to prepare and characterize the same NBF1 segments described above, i.e., P-67 and MBP-NBF1 but lacking phenylalanine 508. The following peptide called P-66 lacking F508 was prepared first employing a peptide synthesizer (model 430 A, Applied Biosystems, Inc., Foster City, CA) using again the

same solid phase method used for P-67 (Thomas et al., 1991). No obvious problems were encountered in either the synthesis or subsequent reverse phase HPLC purification of P-66. A product judged >95% pure by SDS-PAGE, HPLC, amino acid, and sequence analysis was obtained. The yield was 6–10 mg from the crude starting material, in the same range as that obtained for the P-67 wild-type peptide. MBP-NBF1 lacking F508 was then prepared by PCR using the C-1-1/5 clone as the template (Ko et al., 1993). The fusion protein after overexpression in *E. coli*, was purified to apparent homogeneity on an amylose column. The yield of (ΔF508) MBP-NBF1 was ~25 mg/liter of cell culture, in the same range as that obtained for the MBP-NBF1 wild-type protein. The P-66 peptide lacking F508 and the (ΔF508) MBP-NBF1 construct were then analyzed in detail for structural and functional differences from the wild-type proteins.

P-66, physical characterization. The circular dichroism spectra presented in Fig. 4 *A* show clearly that the P-66 peptide bearing the ΔF508 mutation has less ordered structure than the wild-type P-67 peptide. Deconvolution of the two spectra using four different programs (Thomas et al., 1992*b*) indicated that deletion of F508.

TABLE II
Relative Secondary Structural Elements of NBF1 and NBF2 Components
of CFTR as Determined by Circular Dichroism Spectroscopy

CFTR component	Region	Secondary structural element*		
		α helix	β strand	Other†
		% of total		
P-67 from NBF1	R450 → R516	<10	80	10–15
MBP-NBF1	F433 → S589	40	24	36
P-51 from NBF2	E1228 → T1278	20–28	6–11	61–74

*Deconvolution of the spectral data was carried out using the Prosec program.
†Random coil + turns.
See Ko et al. (1993, 1994) and Thomas et al. (1991) for details.

from P-67 to give P-66 is accompanied by a loss of β-sheet secondary structure and a corresponding gain of random coil. Significantly, four different programs for predicting secondary structure indicate that F508 lies within a β-strand region (Thomas et al., 1991). Therefore, one of the simplest interpretations of these studies is that deletion of F508 destabilizes a β-sheet structure and unfolding occurs.

The circular dichroism experiments were reproduced in many different experiments and at many different dilutions of P-66 and P-67, and suggested that deletion of F508 produces a less stable peptide. For this reason we examined the effect of urea on the folding of P-67 and P-66, a study which revealed that the P-66 peptide bearing the F508 mutation unfolds (half maximally) at a significantly lower urea concentration (Fig. 4 *B*). In other studies not presented here, we have shown also that the P-66 peptide unfolds (half maximally) at a temperature 17° below that of P-67.

P-66, ATP binding. P-66 binds TNP-ATP as well as the wild-type peptide P-67. Thus, the localized disruption of structure within the F508 region evidently has little or no effect on the ATP binding region containing the Walker A consensus.

However, when nucleotide binding is measured in the presence of 4 M urea the wild-type peptide retains significant TNP-ATP binding capacity while the mutant peptide has lost this function (Thomas et al., 1992). It will be noted in Fig. 4 *B* that at 4 M urea the P-67 peptide retains about one third of its original secondary structure while the P-66 peptide is completely unfolded.

In other studies we found no detectable capacity for these peptides to catalyze the hydrolysis of ATP.

Model. The structural and functional studies on the wild-type P-67 and mutant P-66 peptides led us to consider the chemical and structural events that may take place when F508 is deleted from a β sheet region of CFTR. As illustrated in Fig. 5, one possibility is that a register shift will occur requiring reorientation of some amino acid side chains from one face of the β sheet to the other. Alternatively, a "β bulge" could form maintaining the residues on each face of the β sheet. Finally, neither of these new structures may be as stable as the original structure and, thus, will not spontaneously fold under physiological conditions. We believe that the latter possibility is most consistent with our structural and functional studies.

TABLE III
Relative Nucleotide-binding Properties of NBF1 and NBF2 Components of CFTR

CFTR component	Region	Dissociation constant (K_d) for ATP	Nucleotide specificity
		mM	
P-67 from NBF-1	R450 → R516	0.59	TNP-ATP > TNP-ADP > TNP-AMP
MBF-NBF1	F433 → S589	1.80	TNPATP > TNP-ADP > TNP-AMP
P-51 from NBF2	E1228 → T1278	0.46	TNP-ATP > TNP-ADP > TNP-AMP

See Ko et al. (1993, 1994) and Thomas et al. (1991) for details.

Hypothesis. Early studies on the membrane trafficking of intact CFTR within the cell were at first puzzling. Some investigators reported that the ΔF508 mutant protein underwent biosynthetic arrest and failed to travel to the plasma membrane (Rich, Anderson, Gregory, Cheng, Paul, Jefferson, McCann, Klinger, Smith, and Welsh, 1990; Anderson, Rich, Gregory, Smith, and Welsh, 1991; Denning, Ostegaard, and Welsh, 1992), whereas other workers reported that the mutant protein does travel to the plasma membrane in functional form (Li, Ramjeesingh, Reyers, Jensen, Chang, Rommens, and Bear, 1993; Drum, Wilkinson, Smit, Worrell, Strong, Frizzell, Dawson, and Collins, 1991). Our studies on purified components, which showed that the ΔF508 mutant peptide (P-66) is less stable, led us to propose that protein unfolding may be the molecular basis of most cases of cystic fibrosis (Thomas, Ko, and Pedersen, 1992*b*). Thus, we suggested that at 37° the ΔF508 mutant protein may be unstable and undergo biosynthetic arrest in some animal cells because of the inability to fold into a compact structure whereas at 27°, i.e., in insect cells (Sf9), the mutant protein may be able to refold into a stable functional protein and travel to the plasma membrane. (In the latter case, it is predicted that deletion of F508 would be

accompanied by the formation of a "remodeled" β-sheet region, two possibilities of which are illustrated in Fig. 5).

Consistent with the above hypothesis Denning, Anderson, Amara, Marshall, Smith, and Welsh (1992) demonstrated that reduced temperature facilitates the processing of the ΔF508 CFTR in 3T3 fibroblasts and C127 cells, resulting in the appearance of cAMP-regulated Cl- channels in the plasma membrane. In a subsequent review (Thomas and Pedersen, 1993), we called attention to the possible use of chaperones in the treatment of cystic fibrosis.

(ΔF508) MBP-NBF1, physical and functional characterization. In a thorough study (Ko et al., 1993) we found no obvious differences in the physical and functional properties of wild-type MBP-NBF1 and (ΔF508) MBP-NBF1. These studies included (*a*) Secondary structural analysis by circular dichroism spectroscopy; (*b*) Susceptibility to protease digestion; (*c*) TNP-ATP binding and its competitive displacement by ATP; (*d*) Effect of urea on the nucleotide binding function; (*e*) HPLC molecular sieve chromatography; and (*f*) Propensity to form polymeric structures and microcrystals.
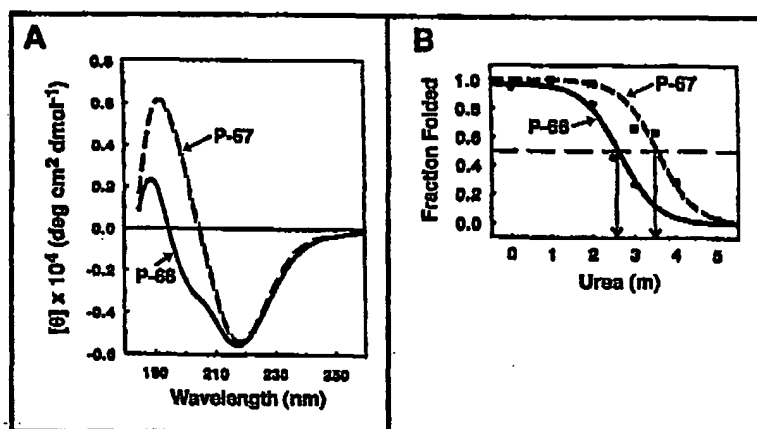

Figure 4. (*A*) Comparison of the circular dichroism spectra of the wild type and P-66 peptides indicating differences in secondary structure. The mean residue molar ellipticity is plotted vs wavelength (reprinted with permission, *Journal of Bioenergetics and Biomembranes*). (*B*) Comparison of the unfolding patterns of P-67 and P-66 in urea based on changes in the mean residue molar ellipticity at 218 nm and reflecting clear differences in the relative stabilities of the two peptides. (for details see Thomas et al., 1992*b*; Thomas and Pedersen, 1993).

These studies together with the additional finding that the maltose binding protein remains associated with NBF1 or ΔF508-NBF1 even after cleavage of the fusion junction, indicates that the obvious structural, stability, and functional differences between mutant and wild-type domains observed for the P-67 and P-66 peptides are not evident. This apparent discrepancy may be explained when one considers that P-67 and P-66 may represent folding intermediates on the pathway toward the native state while the MBP-NBF1 fusion proteins might be the finally folded structures in which the presence of one deleted amino acid fails to make a large difference. Therefore, if one were to obtain a crystal structure of the fusion

proteins described here, it may be possible to deduce the minimal structural change that occurs when ΔF508 is deleted. We intend to work toward this goal.

Findings briefly summarized above are significant for several reasons. First, studies with P-67 and P-66 provided the first experimental evidence indicating that the major cystic fibrosis causing mutation, ΔF508, alters the structure and stability of NBF1. Secondly, these studies provide chemical insight into those changes that may take place in NBF1 when F508 is deleted. Thirdly, MBP or other proteins may be
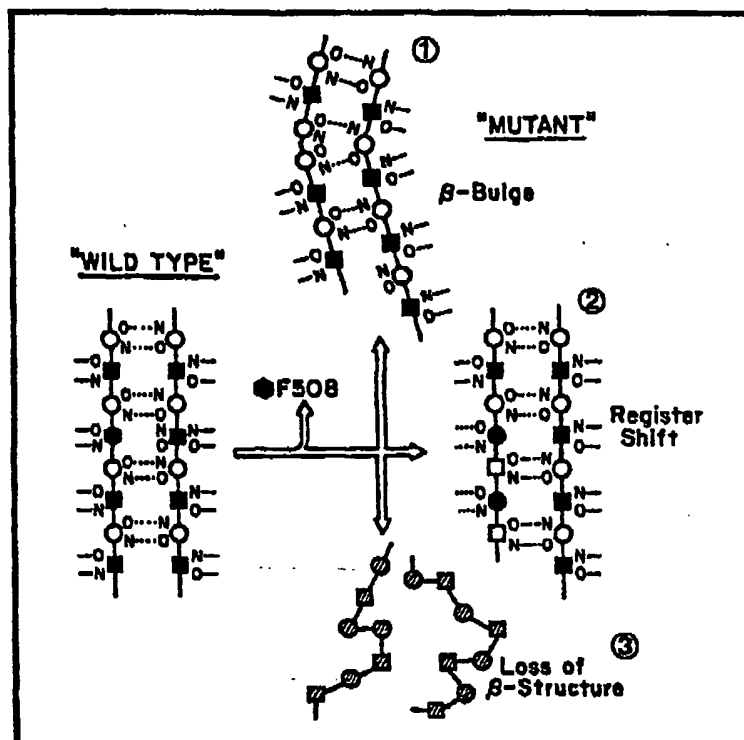

Figure 5. The possible effects of deleting F508 from a β-sheet region. (reprinted with permission from the *Journal of Biological Chemistry*). The β sheet may reform into either structure 1 or 2. However, if the latter are not thermodynamically stable structures, they would not form as depicted in 3. The experimental data obtained on the P-66 peptide relative to the control P-67 peptide indicate that possibility 3 is correct (Thomas et al., 1992*b*).

considered to minimize the effect of the deletion of F508 so that the mutant protein is more similar to that of the wild-type protein. Finally, studies with the MBP-NBF1 and (ΔF508) MBP-NBF1 fusion proteins have provided the first CFTR systems to date amenable to crystallization.

Other studies in progress. The folding pathway of CFTR is being studied in greater detail to define those components of the cell involved in this process. Also,

studies are being conducted to establish whether NBF1 exhibits the capacity to hydrolyze ATP and to interact with biological membranes.

Acknowledgments

References

Anderson, M.P., H. A. Berger, D. P. Rich, R. J. Gregory, A. E. Smith, and M. J. Welsh. 1991. Nucleoside triphosphates are required to open the CFTR chloride channel. *Cell.* 67:775–784.

Anderson, M.P., D. P. Rich, R. J. Gregory, A. E. Smith, and M. J. Welsh. 1991. Generation of cAMP-activated chloride currents by expression of CFTR. *Science.* 251:679–682.

Arispe, N., E. Rojas, J. Hartman, E. J. Sorscher, and H. B. Pollard. 1992. Intrinsic anion channel activity of the recombinant first nucleotide binding fold of the cystic fibrosis transmembrane conductance regulator protein. *Proceedings of the National Academy of Sciences, USA.* 89:1539–1543.

Baichwal, V., D. Liu, and G. F.-L. Ames. 1993. The ATP-binding component of a prokaryotic traffic ATPase is exposed to the periplasmic (external) surface. *Proceedings of the National Academy of Sciences, USA.* 90:620–624.

Cheng, S. H., D. P. Rich, J. Marshall, R. J. Gregory, M. J. Welsh, and A. E. Smith. 1991. Phosphorylation of the R domain by cAMP-dependent protein kinase regulates the CFTR chloride channel. *Cell.* 66:1027–1036.

Chuang, W.-J., A. G. Gittis, C. Abeygunawardana, P. L. Pedersen, and A. S. Mildvan. 1995. Solution structure of the metal-ATP-complex of PP-50 an ATP-binding peptide from F1-ATPase. *Archives of Biochemistry and Biophysics.* In press.

Denning, G., M. P. Anderson, J. F. Amara, J. Marshall, A. E. Smith, and M. J. Welsh. 1992. Processing of mutant cystic fibrosis transmembrane conductance regulator is temperature-sensitive. *Nature.* 358:761–764.

Denning, G.M., L. S. Ostedgaard, and M. J. Welsh. 1992. Abnormal localization of cystic fibrosis transmembrane conductance regulator in primary cultures of cystic fibrosis airway epithelia. *Journal of Cell Biology.* 118:551–559.

Doige, C. A., and G. Ferro-Luzzi Ames. 1993. ATP-dependent transport systems in bacteria and humans: relevance to cystic fibrosis and multidrug resistance. *Annual Review of Microbiology.* 47:291–319.

Drumm, M. L., D. J. Wilkinson, L. S. Smit, R. T. Worrell, T. V. Strong, R. A. Frizzell, D. C. Dawson, and F. S. Collins. 1991. Chloride conductance expressed by ΔF508 and other mutant CFTRs in *Xenopus* oocytes. *Science.* 254:1797–1800.

Fry, D. C., S. A. Kuby, and A. S. Mildvan. 1986. ATP-binding site of adenylate kinase: mechanistic implication of its homology with *Ras*-encoded p21, F1-ATPase, and other nucleotide binding properties. *Proceedings of the National Academy of Sciences, USA.* 83:907–911.

Garboczi, D.N., J. H. Hullihen, and P. L. Pedersen. 1988. Mitochondrial ATP synthase:

overexpression in *Escherichia coli* of a rat liver β-subunit peptide and its interaction with adenine nucleotides. *Journal of Biological Chemistry.* 263:15694–15698.

Garboczi, D.N., P. J. Thomas, and P. L. Pedersen. 1990. Rat liver mitochondrial ATP synthase. Effects of mutations in the glycine-rich region of a β-subunit peptide on its interaction with adenine nucleotides. *Journal of Biological Chemistry.* 265:14632–14637.

Higgins, C.F. 1992. ABC transporters: from microorganisms to man. *Annual Review of Cell Biology.* 8:67–113.

Hyde, S., P. Emsley, M. J. Hartshorn, M. M. Mimmack, U. Gileadi, S. R. Pearce, M. P. Gallagher, D. R. Gill, R. E. Hubbard, and C. F. Higgins. 1990. Structural model of ATP-binding proteins associated with cystic fibrosis, multidrug resistance, and bacterial transport. *Nature.* 346:362–365.

Kerem, E., M. Corey, B. S. Kerem, J. Rommens, D. Mariewicz, H. Levison, H., L.-C. Tsui, and P. Durie. 1990. The relationship between genotype and phenotype in cystic fibrosis analysis of the most common mutation (ΔF508). *New England Journal of Medicine.* 323:1517–1522.

Ko, Y.H., P. J. Thomas, and P. L. Pedersen. 1994. The cystic fibrosis transmembrane conductance regulator: nucleotide binding to a synthetic peptide segment from the second predicted nucleotide binding fold. *Journal of Biological Chemistry.* 269:14584–14588.

Ko, Y.H., P. J. Thomas, and P. L. Pedersen. 1993. The cystic fibrosis transmembrane conductance regulator: overexpression, purification, and characterization of wild-type and F508 mutant forms of the first nucleotide binding fold in fusion with the maltose-binding protein. *Journal of Biological Chemistry.* 268:24330–24338.

Lee, J. H., D. N. Garboczi, P. J. Thomas, and P.L. Pedersen. 1990. Mitochondrial ATP synthase: cDNA cloning, amino acid sequence, overexpression, and properties of the rat liver β subunit. *Journal of Biological Chemistry.* 265:4664–4669.

Li, C., M. Ramjeesingh, E. Reyers, T. Jensen, X. Chang, J. M. Rommens, and C. E. Bear. 1993. The cystic fibrosis mutation (ΔF508) does not influence the chloride channel activity of CFTR. *Nature Genetics.* 3:311–316.

Mildvan, A. S. 1989. Studies of the interaction of substrates with enzymes and their peptide fragments. *FASEB Journal.* 3:1705–1714.

Pedersen, P. L., and L. M. Amzel. 1993. ATP synthases: structure, reaction center, mechanisms, and regulation of one of nature's most unique machines. *Journal of Biological Chemistry.* 268:9937–9940.

Rich, D. P., M. P. Anderson, R. J. Gregory, S. H. Cheng, S. Paul, D. M. Jefferson, J. D. McCann, K. W. Klinger, A. E. Smith, and M. J. Welsh. 1990. Expression of cystic fibrosis transmembrane conductance regulator corrects defective chloride channel regulation in cystic fibrosis airway epithelial cells. *Nature.* 347:358–363.

Riordan, J. R., J. M. Rommens, B. Kerem, N. Alon, R. Rozmahel, Z. Grzelczak, J. Zielenski, S. Lok, N. Plausic, and J. L. Chow. 1989. Identification of the cystic fibrosis gene: cloning and characterization of complementary DNA. *Science.* 245:1066–1073.

Sachsenheimer, W., and G. E. Schulz. 1977. Two conformations of crystalline adenylate kinase. *Journal of Biological Cemistry.* 114:23–36.

Schulz, G.E., M. Elzinga, F. Marx, and R. H. Schirmer. 1974. Three-dimensional structure of adenylate kinase. *Nature.* 250:120–123.

Shyamala, V., V. Baichwal, E. Beall, and G. F. Ames. 1991. Structure function analysis of the

histidine permease and comparison with cystic fibrosis mutations. *Journal of Biological Chemistry*. 266:18714–18719.

Smit, L.S., D. J. Wilkinson, M. K. Mansoura, F. S. Collins, and D. C. Dawson. 1993. Functional roles of the nucleotide-binding folds in the activation of the cystic fibrosis transmembrane conductance regulator. *Proceedings of the National Academy of Sciences, USA*. 90:9963–9967.

Story, R.M., and T. A. Steitz. 1992. Structure of the RecA protein-ADP complex. *Nature*. 355:374–376.

Tabcharani, J. A., X. -B. Chang, J. R. Riordan, and J. W. Hanrahan. 1991. Phosphorylation-regulated Cl⁻ channel in CHO cells stably expressing the cystic fibrosis gene. *Nature*. 352:628–631.

Thomas, P.J., and P. L. Pedersen. 1993. Effects of the ΔF508 mutation on the structure, function, and folding of the first nucleotide-binding domain of CFTR. *Journal of Bioenergetics and Biomembranes*. 25:11–19.

Thomas, P. J., D. N. Garboczi, and P. L. Pedersen. 1992*a*. Mutational analysis of the consensus nucleotide binding sequences in the rat liver mitochondrial ATP synthase β-subunit. *Journal of Biological Chemistry*. 267: 20331–20338.

Thomas, P.J., Y. H. Ko., and P. L. Pedersen. 1992*b*. Altered protein folding may be the molecular basis of most cases of cystic fibrosis. *FEBS Letters*. 312:7–9.

Thomas, P.J., P. Shenbagamurthi, J. Sondek, J. M. Hullihen, and P. L. Pedersen. 1992. The cystic fibrosis transmembrane conductance regulator: effects of the most common cystic fibrosis-causing mutations on the secondary structure and stability of a synthetic peptide. *Journal of Biological Chemistry*. 267:5727–5730.

Thomas, P.J., P. Shenbagamurthi, X. Ysern, and P. L. Pedersen. 1991. Cystic fibrosis transmembrane conductance regulator: nucleotide binding to a synthetic peptide. *Science*. 251:555–557.

Tsui, L.-C. 1992. The spectrum of cystic fibrosis mutations. *Trends in Genetics*. 8:392–398.

Walker, J.E., M. Saraste, M. J. Runswick, and N. J. Gay. 1982. Distantly related sequences in the α- and β-subunits of ATP synthase, myosin, kinases, and other ATP-requiring enzymes and a common nucleotide binding fold. *EMBO Journal*. 1:945–951.